Correlation Effects in EOM-CCSD for the Excited States: Evaluated by AIM Localization Index (LI) and Delocalization Index (DI)

Yi-Gui Wang,*,† Kenneth B. Wiberg,† and Nick H. Werstiuk‡

Department of Chemistry, Yale University, New Haven, Connecticut 06520-8107, and Department of Chemistry, McMaster University, Hamilton, Ontario, L8S 4M1, Canada

Received: November 15, 2006; In Final Form: March 12, 2007

We have extended the evaluation and interpretation of QTAIM (quantum theory of atoms in molecules) localization and delocalization indices λ (LI) and δ (DI) to electronic excited states by studying ground states (at HF and CCSD levels) and excited states (at CIS and EOM-CCSD) of $H_2C{=}CH_2$, $HC{\equiv}CH$, $H_2C{=}O$, $H_2C{=}S$, CO_2, CS_2, and SO_2. These molecules undergo extensive geometrical changes upon the excitation to the valence adiabatic excited singlet state. The importance of Coulomb correlation effects was demonstrated by comparing the LIs and DIs at none-correlated levels (HF and CIS) and those at correlated levels (CCSD and EOM-CCSD). In interpreting the changes in the magnitudes of the LIs and DIs, we made use of simple molecular orbital and Walsh-diagram analyses. Coulomb correlation is important in determining the magnitude of the LIs and DIs and obtaining geometries that are close to experiment.

1. Introduction

Adiabatic electronic excited states (AESs) often have quite different geometries than the corresponding ground states. For example, the $\pi\rightarrow\pi^*$ singlet AES of ethene is twisted[1] and the $n\rightarrow\pi^*$ AES of formaldehyde has a pyramidal geometry.[2] Excited states are traditionally studied with CASSCF and CASPT2 or with more computationally demanding MRCI levels of theory—natural choices because it is necessary to use multiconfiguration methods to accurately describe excited states. However, considerable involvement of the end-user is required in order to correctly set up these calculations and obtain useful results. Single-reference methods such as CIS,[3] TD−DFT,[4] and EOM-CCSD[5] are more user-friendly. CIS is based on HF, so no Coulomb correlation (CC) is included. EOM-CCSD includes Coulomb correlation through the robust CCSD approach and has been successfully used in studying excited states. TD−DFT is used extensively for large systems because DFT methods are less resource-demanding. In principle, wave functions required for QTAIM (quantum theory of atoms in molecules)[7] analyses can be generated at all these levels of theory.

A rigorous analysis of the density with QTAIM that defines atoms in physical space—atoms defined in this way satisfy all quantum principles—provides a unique way to study chemical bonding and electron delocalization of any chemical species. The localization index λ (LI) and delocalization index δ (DI) are two parameters among the wide variety of QTAIM-derived tools that are available for analyzing bonding based on concepts which mesh with current chemical thinking.[8,9] One obvious advantage is that the sum given in eq 1 that includes the LIs (λ_i) and DIs (δ_{ij}) equals the total number of electrons N of the system where n is the number

$$N = \sum_i^n \lambda_i + \frac{1}{2}\sum_{i\neq j}^n \delta_{ij} \tag{1}$$

of atoms. The key points are that the magnitude of the DI is close to the conventional covalent bond order at HF level and the DI is related to the shared pair density between two atoms,[10] so the percent pair delocalization can be calculated for any pair of atoms in a molecule.[9] These concepts established at HF level of theory have been extended to the framework of the two reduced density matrix (2RDM) at the CISD level.[11] Several years ago, we proposed to use the following equations to calculate LI and DI at post-HF levels of theory within the framework of one reduced density matrix (1RDM):[12]

$$\lambda(A,A) = \sum_{l,m} n_l^{1/2} n_m^{1/2} S_{lm}(\Omega_A) S_{lm}(\Omega_A) \tag{2}$$

$$\delta(A,B) = 2\sum_{l,m} n_l^{1/2} n_m^{1/2} S_{lm}(\Omega_A) S_{lm}(\Omega_B) \tag{3}$$

In eqs 2 and 3, the n values are occupation numbers of natural orbitals, and the $S_{lm}(\Omega)$ values are atomic overlap matrix elements, with Ω denoting the real space of the QTAIM atomic basin. The l and m stand for natural spin orbitals. The starting natural orbitals are obtained by GAUSSIAN packages at post-HF levels of theory.

The idea to use eqs 2 and 3 to evaluate electron sharing was proposed by Fulton.[13] Equations 2 and 3 are generally considered to be only applicable at the HF level since the idea is based on single determinant. Our study was undertaken (a) to establish the importance of Coulomb correlation (CC) in determining the magnitudes of LI and DI and (b) to evaluate the various currently used correlated methods, keeping in mind that correlation energy usually is a small part of the total energy. The comparison between 2RDM CISD results[11] and those we calculated with eqs 2 and 3 at the same level showed promising agreement,[12a] so we evaluated Coulomb correlation effects (CCEs) with conventional correlation methods (MP2, MP4(SDQ), CISD,

* Corresponding author. E-mail: yi-gui.wang@yale.edu.
† Yale University.
‡ McMaster University.

10.1021/jp067579t CCC: $37.00
Published on Web 04/19/2007

QCISD).[12b] These methods are available in the GAUSSIAN packages and are used extensively to study ground state properties of molecules.

Both CCEs and electronic excited states make use of excited determinants. While CCEs are most accurately included in configuration interaction (CI) calculations, full CI calculations which include all possible configurations are only practical for small molecules. Consequently CCEs are approximated by a large number of post-HF methods,[44,53−54] among which CISD has conceptual advantages. The first density analyses at correlated levels were carried out using CISD and MP2,[55] and the first evaluation of LIs and DIs at CISD was documented a few years later.[11] The generalization of the procedure to include CCEs in the calculation of LIs and DIs was also made.[10,45] The 2RDM problem also initially rendered geometry optimizations at all correlated levels problematic. The breakthrough came in the 1980s through the development of the *Z*-vector method for evaluating post-HF derivatives[56] with wave functions based on the relaxed density being written in terms of a complete set of natural orbitals. Although natural orbitals were first used to evaluate the effect of Coulomb correlation on the density distribution in 1988,[66] these wave functions were first used in ground state density analyses at conventional correlated levels in 1992.[57] Given that the key requirement is the evaluation of post-HF derivatives, it was eventually possible to study excited states at the CIS level.[3,6,46,58] While post-HF derivatives are available for CCSD in GAUSSIAN 03,[67] this is not the case for EOM-CCSD required for studying excited states. Nevertheless, ACES II[14] has this capability.

We previously studied the adiabatic excited states (AESs) of eight small molecules at the CIS and EOM-CCSD levels and showed that CIS optimized geometries are good starting points for more expensive EOM-CCSD calculations. The good performance of CCSD (for ground states) and EOM-CCSD (for excited states) led us to study CCEs in the excited sates of $H_2C{=}CH_2$, HC≡CH, $H_2C{=}O$, $H_2C{=}S$, CO_2, CS_2, and SO_2 through evaluation of LIs and DIs. The detailed studies at CIS level (including the study of covalent bond orders) on ethene and formaldehyde were published 15 years ago.[58] For the purpose of comparison we also studied excited states of these molecules at the CIS level. As far as we are aware, this is the first general LI-DI study of excited states at both CIS and EOM-CCSD levels. Although the concept of LI and DI are employed here, they are identical to other definitions in the family of electron sharing index with 1RDM.[50,51] Some relevant studies on singlet and triplet H_2 have also been reported.[59,61]

In this paper we report and discuss the results of our studies (a) on the excited states at the CIS and EOM-CCSD levels and (b) comment on the validity to evaluate LIs and DIs at correlated levels of theory in the framework of 1RDM.

2. Methods

To compare the performances of the methods, we optimized ground states at the HF and CCSD levels and excited states at the CIS and EOM-CCSD levels using the 6-311++G(d,p) basis set. All MOs are active in CCSD and EOM-CCSD calculations. The 6-311++G(d,p) basis set is sufficient because the species we investigated are valence excited states—more flexible diffuse functions are necessary for studying Rydberg states.[47] Then the CCSD and EOM-CCSD structures are used to evaluate LIs and DIs; HF and CIS LIs and DIs were calculated with the corresponding CCSD and EOM-CCSD structures to avoid the difference introduced by the geometries. A modified version of ACES-II[14] that generates natural molecular orbitals (NMOs) corresponding to the relaxed density of the EOM-CCSD excited states was used to obtain wave functions in the GAUSSIAN format. The latter, as described in our paper,[6] is the basis of our current density analyses at CCSD and EOM-CCSD levels. The procedure was calibrated by comparing the ground state wave functions obtained with ACES II natural orbitals and those directly written by Gaussian at CCSD level.

Due to the concerns about the validity of using 1RDM to include CCE, we make important points discuss a little more in the following three paragraphs. It is instructive to review the nature of the wave functions obtained at HF and correlated levels. For example, ethene has 74 basis functions with 6-311++G(d,p) basis set from which 74 MOs are constructed by the LCAO procedure.[52] In the case of HF, the first 8 MOs span the single-determinant space and the remaining 66 virtual MOs are not used. All 74 MOs are used in the correlated methods (CCSD, EOM-CCSD) and CIS. In practice, the derivatives (including gradients) are calculated in the HF basis. This resulting density is non-diagonal and represents combinations of HF orbitals. It also departs from a simple occupation number analysis. So at the end of the calculation, the correlated density is diagonalized to provide natural orbitals and a diagonalized correlated density matrix.[65] We will prove in this paper that the occupation of the HF virtual space is the reason why CCE is included in 1RDM. Although the partition of physical space can be done in different ways, we are not aware of other simpler ways to get density at correlated levels than the post-HF derivative approach. The diagonal step will ensure that the sum of natural MO occupation numbers is equal to the total number of electrons. The single determinant recovers the property of Fermions and its "enlarged" size with natural occupation numbers allows for the inclusion of Coulomb correlation. Although some MOs in the virtual MO space are more important than others—as, for example, the π^* MO in our case—small contributions from other MOs cannot be ignored.[68] Ponec and Cooper demonstrated the usefulness of their domain-averaged Fermi hole analysis at correlated levels, but the sum of occupation numbers of natural orbitals is not equal to the total number of electrons.[62]

Buijse's et al.[49] showed that it was possible to include CCEs in the 1RDM and this is realized through evaluation of post-HF derivatives for conventional correlated methods to study both ground states and excited states. For example, in the case of CIS, a determination of post-HF derivatives allows for the evaluation of the generalized density matrix (1RDM)—with core Hamiltonian derivatives—and the 2 density matrix (2RDM)—with AO derivative integrals—along with the energy gradient.[46] A natural-orbital functional theory as an alternative to DFT has been advocated and is being investigated by Cioslowski.[48,63]

While AIMALL was used to obtain most of the atomic overlap matrices,[15] in some cases PROAIMV of AIMPAC[16] was used to increase the accuracy of the integrations for some excited states because the electron density is much more diffuse in excited states than in ground states. LIs and DIs were calculated by LI-DICALC.[17]

Walsh diagrams were constructed at the HF/6-311++G(d,p) level, and MO plots were made with the CASGEN program.[64] Walsh initially used simple orbital arguments to explain the molecular distortions in the excited states.[25] It has been shown that trends in the shapes of bending potential energy curves at self-consistent field (SCF) level of treatment can generally be predicted on a reliable basis with the aid of Walsh's qualitative theory.[42]

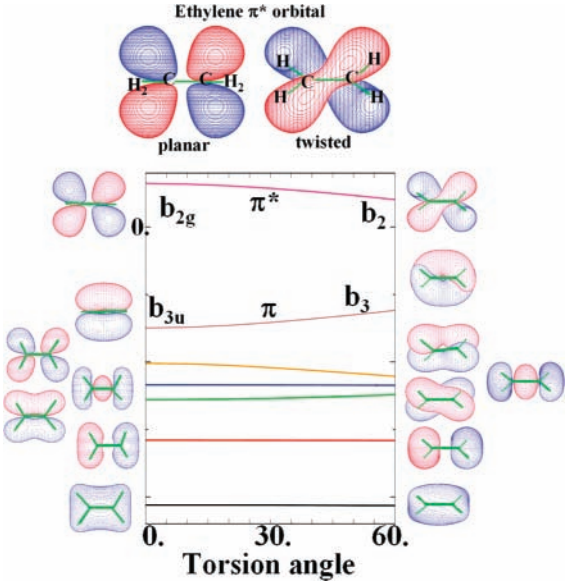

Figure 1. Ethene π^* molecular orbitals and Walsh diagram.

3. Results

3.1. $\tilde{A}^1B_{1u}$ ($\pi\rightarrow\pi^*$) Excited State of Ethene. The ground state of ethene is planar, with the experimental C−C bond length being 1.339 Å.[18] The optimized C−C bond lengths are 1.319 and 1.337 Å at the HF/6-311++G(d,p) and CCSD/6-311++G-(d,p) levels, respectively, clearly showing that the HF C−C bond length is too short. On the basis of the CCSD structure, CCSD yields a DI of 1.491 that is much smaller than the HF DI of 1.884. In order to have some idea about other conventional correlated methods,[12b] we repeated the calculations with QCISD method. With the same geometry, QCISD/6-311++G(d,p) gives a similar DI of 1.488. The ρ_{BCP} values (density at C−C bond critical point) are 0.347, 0.337, and 0.337 e.a_0^{-3} at HF level, CCSD level, and QCISD level, respectively. The agreement between CCSD and QCISD is remarkable. The complete QCISD results can be found in Table S3. This CCE is generally seen in multiple bond DIs obtained by conventional correlated methods,[11,12,50] but 1.491 is much smaller than the value of 2 that is expected for a covalent double bond. The reason for this result is discussed later.

The EOM-CCSD optimized C−C bond length (1.344 Å) of the AES is shorter than the CIS one (1.373 Å). While the CIS value is closer to the experimental value of ~1.4 Å than the EOM-CCSD value, it is possible that the experimental C−C bond length is in error given that the H−C−C−H torsional angle is very uncertain (37−90°). This is the only case in our study that CIS gives longer bond length than EOM-CCSD. Apparently, the degeneracy of two states for 90°-rotated structure attributes to this unusual result. For the $\pi\rightarrow\pi^*$ excitation, one electron is promoted from the bonding π MO to π^*. The classical Lewis structure representation would show the π electrons localized on individual carbon atoms—in two separated carbon basins. If these electrons are considered to exhibit Coulomb repulsion, a rotation about the C−C bond could, in principle, reduce the repulsion.[43] This rotation could also reduce the repulsion between the bonding pairs of the in-plane CH_2 groups. The Walsh diagram (Figure 1) predicts that the energy of the π^* MO decreases during the rotation while the energy of the π MO increases. There is a stabilization of HOMO-1 (orange line) that has π-CH_2 character. That the twisted geometry is the low energy state may derive from the decrease of the repulsive interactions or a favorable delocalization stabilization between the C−H's and remote partially occupied orbitals,[20] as shown schematically in Figure 2.

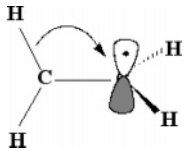

Figure 2. Schematic representation of delocalization.

The driving force for the structure change is related to π^* MOs and those MOs interacting with it. In studying LIs and DIs in open-shell molecules, Fradera and Sola showed that $\pi-\sigma$ and α, β spin contributions to LIs and DIs could be evaluated in molecules of high symmetry.[59c] We can separate $\pi-\sigma$ but do not intend to separate α, β spin contributions because of the NMOs with fractional occupation numbers in our calculations. The triplet excited states have quite different structures, and we focus on the singlet $\pi\rightarrow\pi^*$ state here. A detailed study on the excited states of ethene at CIS level has been documented in 1992, which carefully studied a large number of singlet and triplet excited states.[58a] That study also reported the covalent bond orders for the excited states, including the separated contributions from $\sigma-\pi$ components.

The basic features based on π^* molecular orbital and Walsh diagram are confirmed by LIs and DIs (Table 1). Going to the $\pi\rightarrow\pi^*$ vertical excited state (VES), the C−C DI values are significantly reduced, while the C LIs are increased. The changes at CIS level are about twice as large as those at the EOM-CCSD level. On going to the relaxed adiabatic excited state (AES), the C−C DI increases at the expense of C−H DIs.

In going from the GS to the VES at CCSD, the C−C DI decreases by 0.325 from 1.491 to 1.166. The occupation numbers for π NMO and π^* NMO change from 1.917 and 0.067 to 1.0378 and 0.935, which is acceptable for a singlet excited state. If changes in the atomic overlap matrices (AOM) corresponding to these two NMOs are not considered, vertical excitation yields a reduction of 0.54 in the C−C DI. If the changes in the AOMs are included, the reduction is 0.46. When all NMOs with π-character are involved, the reduction is 0.41. It is obvious that the occupation number is the most important factor in reducing DIs, with the changes in AOMs narrowing the difference. In our view, this is also the reason why the C−C DI for the GS is much smaller at CCSD (1.491) than at HF (1.884). At the HF level, the π^* MO whose occupation number is 0 does not contribute to the evaluation of the DI. If in the CCSD GS wave function all NMOs in the former HF virtual space except π^* NMO are set unoccupied, the C−C DI increases to 1.611. If the π^* NMO in the CCSD GS wave function is also set unoccupied, the C−C DI increases further to 1.842 (0.26 e missing). This value is very close to the HF value. The important conclusions that can be drawn are (a) that the occupied virtual space in the correlated wave function is the source of the Coulomb correlation effect and (b) π^* NMO is the most important contributor. An interesting fact is that CCSD C−C ρ_{BCP} increases from 0.337 e.a_0^{-3} in GS to 0.348 e.a_0^{-3} in VES (Table S2 and Table S4). This is also true at HF (CIS) level (Table S1 and Table S3). Since the electron density in π bond has a nodal plane along C−C bond (Figure 1), it contributes little to ρ_{BCP} in GS, and the rearrangement of electron density due to $\pi\rightarrow\pi^*$ excitation slightly increases the C−C ρ_{BCP} in VES.

In going from the VES to the twisted AES (EOM-CCSD geometry, whose C−C bond length is only 0.007 Å longer than that in GS), the slight increase in the C−C DI and the decrease of the C−H DI are the results of overlap involving the π NMOs.

TABLE 1: Calculated and Experimental Properties of Ethene Ground State ($\tilde{X}^1A_g$) and $\pi\rightarrow\pi^*$ Excited State ($\tilde{A}^1B_{1u}$)

	GS[a]			vertical excited state[a]		adiabatic excited state		
	expt[18]	HF	CCSD	CIS	EOM	expt[19]	CIS[b]	EOM
C−C	1.339	1.319	1.337			1.4	1.373	1.344
τ[c]	0	0	0			37−90	88.5	87.0
N[d]								
C		−0.004	−0.029	−0.123	−0.140		−0.112	−0.162
H		0.002	0.014	0.062	0.071		0.056	0.081
λ[e]								
C		4.014	4.389	4.471	4.638		4.445	4.658
H		0.446	0.515	0.391	0.446		0.424	0.469
δ[e]								
C−C		1.884	1.491	1.233	1.166		1.350	1.281
C−H		0.982	0.847	0.986	0.869		0.943	0.822
C−H(C2)[f]		0.067	0.048	0.052	0.048		0.051	0.042
H, Hc[g]		0.012	0.010	0.014	0.013		0.005	0.004
H, Ht[g]		0.007	0.006	0.009	0.009		0.005	0.004
$\Sigma\lambda + 0.5\Sigma\delta$		16.001	16.001	16.008	15.994		16.003	15.999

[a] The CCSD structure is used for the calculations of topological properties of the ground state and the vertical excited state. [b] EOM-CCSD structure is used to calculate topological properties with CIS. [c] τ is the H−C−C−H dihedral angle. [d] N is the net atomic charge. [e] λ is the localization index (LI), and δ is delocalization index (DI). [f] The DI between C and H on the other carbon. [g] H's are on two different carbons (c, cis; t, trans).

TABLE 2: Calculated and Experimental Properties of Acetylene Ground State ($\tilde{X}^1\Sigma_g^+$) and $\pi\rightarrow\pi^*$ Excited State ($\tilde{A}^1A_u$)[a]

	GS			vertical excited state		adiabatic excited state		
	expt[21]	HF	CCSD	CIS	EOM	expt[22]	CIS	EOM
C−C	1.208	1.183	1.209			1.375	1.356	1.364
C−H	1.057	1.056	1.066			1.097	1.082	1.099
H−C−C	180	180	180			122.5	124.6	123.6
N								
C		−0.171	−0.152	−0.250	−0.201		−0.093	−0.093
H		0.171	0.152	0.250	0.200		0.093	0.093
λ								
C		4.224	4.608	4.946	4.997		4.793	4.941
H		0.310	0.399	0.257	0.341		0.387	0.465
δ								
C−C		2.862	2.192	1.628	1.491		1.578	1.429
C−H		0.959	0.844	0.946	0.875		0.974	0.826
C−H (C2)		0.072	0.050	0.037	0.037		0.055	0.048
H−H[b]		0.003	0.003	0.003	0.005		0.012	0.011
$\Sigma\lambda + 0.5\Sigma\delta$		13.996	13.997	14.005	13.995		14.006	13.998

[a] Refer to the notes of Table 1 for the meanings of the symbols. [b] H's are on two different carbons.

There are two other occupied NMOs (HOMO-1 and HOMO-3, Figure 1, green line and yellow line). The π NMOs increase the C−C DI by approximately 0.11, and reduce each C−H DI by about half that value. Twisting reduces the antibonding character of π^* and increases the C−C DIs a consequence, perhaps, of type of delocalization shown in Figure 2. In the excited states π and π^* are roughly singly occupied. In the AES, twisting of the CH_2 makes possible delocalization of electrons from the C−H region to the π^* NMO. This conclusion is supported by the changes in the net atomic charges and by the fact the energy of HOMO-1 decreases in going to the AES (Figure 1, yellow line). The ρ_{BCP} values for CC bond separately decrease to 0.343 e.a_0^{-3} and 0.333 e.a_0^{-3} at CIS and EOM-CCSD levels of theory (Table S5 and Table S6), which is possibly the consequence of much longer C−C bond length in AES.

3.2. $\tilde{A}^1A_u$ ($\pi\rightarrow\pi^*$) Excited State of Acetylene. Acetylene is a linear molecule in its GS. While CCSD/6-311++G(d,p) calculations reproduced experimental parameters with good accuracy,[21] the C−C bond length is too short at HF/6-311++G-(d,p) (Table 2). Acetylene has two degenerated π molecular obitals (Figure 3), and excitation of one electron from the π_u (a_u) occupied MO to the π_g (a_g) virtual MO yields the $\tilde{A}^1A_u$ excited state. The overall effect is to 'localize' more electrons on the Cs and reduce the electron density in C−C binding region. A sp → sp2 rehybridization with formation of a trans excited state (Figure 3) would minimize the repulsion between the "localized" electrons.[23,43]

In going from the GS to the VES, the C−C DIs are significantly reduced, while the C LIs are increased (Table 2). As seen in ethene, the C−C DI (2.192) at CCSD is significantly smaller than the HF DI (2.862) (Table 2). The dramatic reduction of the C−C DI at CCSD again derives from the involvement of π^* NMO. With all NMOs in virtual space set unoccupied, the calculated C−C DI is 2.77. There are 0.25e distributed in virtual space. The small charge separation between carbon and hydrogen can be traced to the high s-character in the C−H bond (sp).

Although the EOM-CCSD C−C DI is still smaller than the CIS C−C DI, they are closer together in the VES relative to the GS. In going to the AES, at EOM-CCSD the C−C and C−H DIs decrease while the C LIs increase for AES. The significant increase in C−C bond length is a possible cause of reduced C−C DI and ρ_{BCP}s (Supporting materials). These results are in accord with the lone-pair-like localization of electrons at carbon and the sp → sp^2 rehybridization.

On the whole, CCE will reduce DIs and increase LIs for ground states and excited states. In this regard, it appears that the difference between CIS and EOM-CCSD for the excited states is much smaller than the difference between HF and CCSD for the ground states.

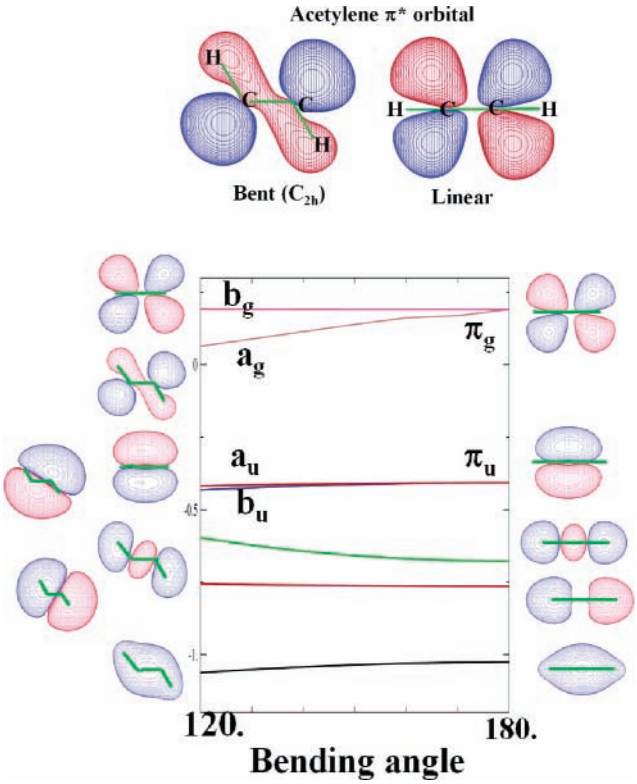

Figure 3. Acetylene π^* molecular orbitals and Walsh diagram.

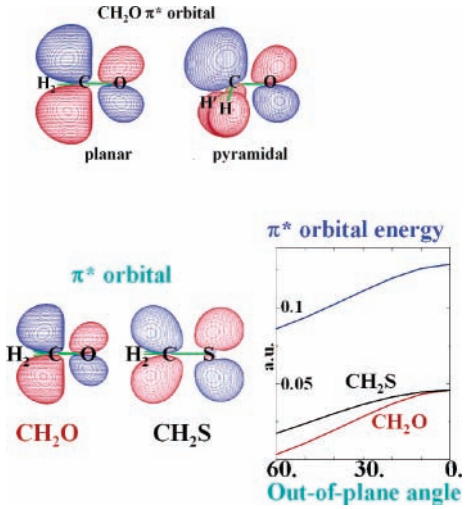

Figure 4. Formaldehyde and thioformaldehyde π^* MOs.

3.3. $\tilde{A}^1A_2$ Excited States of Formaldehyde and Thioformaldehyde. The $\tilde{A}^1A_2$ excited-state is considered to arise via excitation of an electron from an in-plane lone-pair orbital to a π^* MO. Formaldehyde (Table 3) and thioformaldehyde (Table 4) exhibit pyramidal and planar AESs, respectively.[24] If we compare the π^* MOs, formaldehyde has larger coefficients on C than on O; thioformaldehyde has roughly the same-sized coefficients on both C and S (Figure 4). Consequently $n\rightarrow\pi^*$ excitation puts more electrons on C than on O in formaldehyde, while electron density will be roughly equally distributed on C and S in the excited-state of thioformaldehyde. Furthermore, the pryamidalization of the CH_2 group leads to a smaller decrease in energy of the π^* MO of thioformaldehyde than in the case of formaldehyde (Figure 4; the extra line is the actual energy of π^* MO of formaldehyde). For formaldehyde, Walsh suggested that the energy decrease seen when the CH_2 of formaldehyde is pyramidalized derives from mixing s-character into the p-orbital.[25] This locates electrons in an sp^3-like orbital closer to the nucleus; a decrease in kinetic energy "stabilizes" the pyramidal structure.[37]

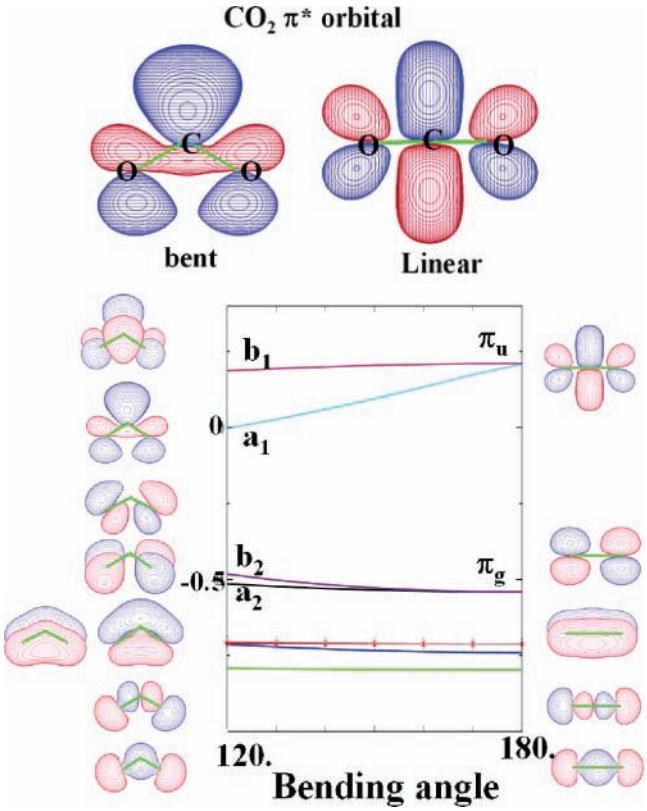

Figure 5. The π^* MO and Walsh diagram for CO_2 (it is used for discussion SO_2 and CS_2).

For formaldehyde, a deformation density plot[6] and an earlier difference projection function[26] study showed an obvious p→p character ($n_y\rightarrow n_x$) on O in the $n_y\rightarrow\pi^*$ VES. In this case, CIS and EOM-CCSD show a decrease in the C−O DIs which indicates that C═O loses covalent double-bond character during the excitation. The C−H DIs increase relative to the GS in going to the VES. These changes are enhanced in the relaxed pyramidal AES. The ionic interaction (C^+O^-) is revealed by the large charge separation. One may refer to reference 58b for detailed studies on the excited states of formaldehyde and acetaldehyde at CIS level. The covalent bond orders including separated π-contributions for many excited states were reported in that study.

One difference between formaldehyde and thioformaldehyde is the net charges on O and S and their LIs (Table 3 and Table 4). Oxygen of formaldehyde loses electrons and exhibits a reduced LI in going to the VES; in the case of thioformaldehyde, S also loses electrons, but LI increases in going to the VES. As seen in the fact that the LI of O decreases and the LI of C increases, additional electron density is transferred from O to C in going to the AES of formaldehyde; this accumulation of electrons on C is in accord with the fact that the AES exhibits a pyramidal geometry. In going from the VES to the AES in the case of thioformaldehyde, the C−S DIs decrease only marginally (simply due to the increase in C−S bond length). This result is in keeping with that fact that it remains planar while exhibiting essentially the same C═S double-bond character in both states.

Again, for the GSs of formaldehyde and thioformaldehyde, the CCSD DIs (1.281 and 1.583) are significantly smaller than HF DIs (1.413 and 2.033), which is due to the partial occupation

TABLE 3: Calculated and Experimental Properties of Formaldehyde (Ground State ($\tilde{X}^1A_1$) and $n_y \rightarrow \pi^*$ Excited State ($\tilde{A}^1A_2$))[a-c]

	GS			vertical excited state		adiabatic excited state		
	expt[27]	HF	CCSD	CIS	EOM	expt[28]	CIS	EOM
C−O	1.203	1.180	1.206			1.323	1.248	1.311
C−H	1.101	1.094	1.106			1.103	1.087	1.096
HCH	116.3	116.2	116.1			118.1	118.2	118.8
α[b]	0	0	0			34	22.5	29.5
N								
C		1.191	1.035	0.576	0.565		0.493	0.494
O		−1.221	−1.066	−0.838	−0.795		−0.703	−0.679
H		0.015	0.015	0.131	0.115		0.111	0.092
λ								
C		3.200	3.548	3.989	4.150		4.094	4.238
O		8.399	8.336	8.239	8.242		8.156	8.166
H		0.451	0.530	0.369	0.455		0.382	0.468
δ								
C−O		1.413	1.281	1.073	1.004		0.986	0.927
C−H		0.903	0.777	0.901	0.783		0.922	0.804
O, H		0.115	0.090	0.067	0.052		0.062	0.050
H, H′		0.050	0.042	0.030	0.025		0.029	0.025
$\Sigma\lambda + 0.5\Sigma\delta$		16.000	16.000	15.999	16.000		15.997	16.000

[a] The meanings of symbols can be found in Table 1. [b] Bending angle α is defined by the angle between a line bisecting HCH angle in the HCH plane and the C−O bond. [c] For the topology analyses, CCSD and EOM-CCSD structures are also used for the corresponding HF and CIS calculation.

TABLE 4: Calculated and Experimental Properties of Thioformaldehyde (Ground State ($\tilde{X}^1A_1$) and $n_y \rightarrow \pi^*$ Excited State ($\tilde{A}^1A_2$))[a-c]

	GS			vertical excited state		adiabatic excited state		
	expt[29]	HF	CCSD	CIS	EOM	expt[30]	CIS	EOM
C−S	1.614	1.596	1.615			1.682	1.637	1.698
C−H	1.096	1.080	1.091			1.077	1.077	1.087
HCH	116.2	115.9	115.9			120.7	118.3	119.7
α[b]	0	0	0			0	0	0
N								
C		−0.606	−0.544	−0.886	−0.690		−0.367	−0.321
S		0.482	0.448	0.733	0.550		0.214	0.177
H		0.061	0.049	0.077	0.071		0.081	0.072
λ								
C		4.620	4.916	5.197	5.232		4.721	4.901
S		14.420	14.697	14.545	14.813		15.089	15.218
H		0.398	0.487	0.388	0.472		0.381	0.468
δ								
C−S		2.033	1.583	1.376	1.204		1.305	1.129
C−H		0.969	0.835	1.001	0.856		0.994	0.856
S−H		0.079	0.063	0.039	0.034		0.050	0.040
H, H′		0.033	0.029	0.030	0.026		0.030	0.026
$\Sigma\lambda + 0.5\Sigma\delta$		24.002	23.995	24.005	23.998		23.996	24.001

[a] The meanings of symbols can be found in Table 1. [b] Bending angle α is defined by the angle between a line bisecting HCH angle in the HCH plane and C−S bond. [c] For the topology analyses, CCSD and EOM-CCSD structures are also used for the corresponding HF and CIS calculations.

of π^* at CCSD level. When all virtual NMOs are set unoccupied, the CCSD DIs increase to 1.498 and 2.002 for formaldehyde and thioformaldehyde, respectively. In the VES, more electrons move into π^*, and the DIs decrease further. Unlike ethene, electrons are promoted from a lone pair orbital rather than from the π NMO.

HF and CIS predict too short C−X bonds for the ground states and excited states of formaldehyde (Table 3) and thioformaldehyde (Table 4). CIS works qualitatively well in modeling the geometrical changes, yet due to the lack of the Coulomb correlation, the C−X bond lengths are too short, bending angles are too small, and DIs are overestimated.

3.4. Excited States of CO_2 and CS_2, and the $\tilde{C}^1B_2$ ($^1A'$) Excited State of SO_2. While the degenerate occupied π_g MOs of CO_2 exhibit the largest coefficients on the oxygen atoms, the virtual $\pi_u(\pi^*)$ MOs have the largest coefficients on carbon (Figure 5). Promotion of an electron into the $\pi_u(\pi^*)$ MO leads to bent AESs for CO_2 and CS_2. Bending CO_2 can put density in an in-plane sp^2-like orbital and lead to a stabilization of the π_u MO (Figure 5).

On the basis of the electronegativities of S and O, the polarization of the multiple bonds of SO_2 should be similar to the polarization of the bonds of CO_2, except that S bears an additional pair of valence electrons. These electrons occupy a π_u MO that exhibits the largest coefficients on S (Figure 5). The Walsh diagram predicts a bent structure—π_u goes to stabilized a_1—for the ground state of SO_2. In going to the $\tilde{C}^1B_2$ ($^1A'$) excited-state an electron is promoted from a_2 to b_1; density is moved from the terminal Os to S. Although a_2 and b_1 are perpendicular to the O−S−O plane, the excitation may reduce repulsion between terminal Os and the increased antibonding character at the central S (also puts more density on S, so more space is required for a_1 and b_1) and lead to an AES that has a smaller O−S−O angle (105°) than the GS (119°) (Table 7). In fact, experimental studies established that this excited-state has unequal S−O bond lengths and the barrier for its degenerate rearrangement is 141 cm^{-1}.[36] At EOM-CCSD, the unsymmetrical $\tilde{C}^1B_2$ ($^1A'$) excited-state is only 19 cm^{-1} lower in energy than the symmetrical one.[6] At a higher level (AQCC/ANO-type basis) the barrier was 170 cm^{-1}.[39] While Mulliken proposed

TABLE 5: Calculated and Experimental Properties of CO_2 (Ground State ($\tilde{X}^1\Sigma_g^+$) and $\pi\rightarrow\pi^*$ Excited State ($\tilde{A}^1A_2$))[a,b]

	GS			vertical excited state		adiabatic excited state		
	expt[31]	HF	CCSD	CIS	EOM	expt[32]	CIS	EOM
C−C	1.164	1.136	1.160			1.262	1.210	1.242
O−C−O	180	180	180			129.0	130.3	129.1
N								
C		2.555	2.255	1.864	1.665		1.771	1.609
O		−1.277	−1.128	−0.931	−0.832		−0.886	−0.804
λ								
C		2.257	2.517	2.991	3.252		3.166	3.384
O		8.519	8.420	8.305	8.256		8.235	8.206
δ								
C−O		1.188	1.174	1.146	1.083		1.063	1.007
O−O′		0.327	0.243	0.105	0.069		0.241	0.189
$\Sigma\lambda + 0.5\Sigma\delta$		21.998	22.002	21.999	21.999		22.003	22.000

[a] The CCSD and EOM-CCSD structures also used to calculate topology properties at HF and CIS levels. [b] The meanings of symbols can be found in Table 1. [c] The data were calculated only from two π NMO (a_2 and lower red line).

TABLE 6: Calculated and Experimental Properties of CS_2 Ground State ($\tilde{X}^1\Sigma_g^+$) and $\pi\rightarrow\pi^*$ Excited State ($\tilde{A}^1A_2$))[a,b]

	GS			vertical excited state		adiabatic excited state		
	expt[33]	HF	CCSD	CIS	EOM	expt[34]	CIS	EOM
C−S	1.559	1.543	1.557				1.600	1.633
S−C−S	180	180	180			135	142.2	138.4
N								
C		−1.309	−1.247	−1.624	−1.666		−1.249	−1.024
S		0.655	0.624	0.813	0.833		0.625	0.512
λ								
C		5.233	5.592	6.135	6.157		5.609	5.639
S		14.116	14.405	14.421	14.356		14.504	14.748
δ								
C−S		2.075	1.655	1.493	1.509		1.638	1.384
S−S′		0.382	0.285	0.043	0.112		0.104	0.094
$\Sigma\lambda + 0.5\Sigma\delta$		37.996	37.997	38.006	38.002		37.997	37.999

[a] The CCSD and EOM-CCSD structures are also used to calculate topology properties at HF and CIS levels. [b] The meanings of symbols can be found in Table 1. [c] The data were calculated only from two π NMO (a_2 and lower red line).

TABLE 7: Calculated and Experimental Properties of SO_2 Ground State ($\tilde{X}^1A_1$) and $\pi\rightarrow\pi^*$ Excited State ($\tilde{C}^1B_2$)[a,b]

	GS			vertical excited state		adiabatic excited state			
	expt[35]	HF	CCSD	CIS	EOM	expt[36]	CIS	EOM[c]	EOM[d]
S−O	1.431	1.408	1.445			1.491	1.515	1.560	1.510
S−O′	1.431	1.408	1.445			1.639	1.515	1.560	1.630
O−S−O	119.3	118.6	118.8				105.3	104.8	104.9
N									
O		−1.289	−1.161	−1.026	−1.001		−0.897	−0.869	−0.905
S		2.579	2.323	2.053	2.003		1.795	1.738	1.683
O		−1.289	−1.161	−1.026	−1.001		−0.897	−0.869	−0.779
λ									
O		8.445	8.421	8.426	8.416		8.310	8.293	8.288
S		12.069	12.456	12.905	12.986		13.195	13.283	13.321
O		8.446	8.421	8.426	8.415		8.310	8.293	8.228
δ									
O−S		1.352	1.221	1.045	1.012		1.013	0.978	1.065
S−O′		1.352	1.221	1.045	1.012		1.013	0.978	0.926
O−O′		0.336	0.258	0.157	0.161		0.163	0.173	0.166
$\Sigma\lambda+0.5\Sigma\delta$		31.999	31.999	32.005	32.000		32.004	31.999	31.995

[a] The CCSD and EOM-CCSD structures also used to calculate topology properties at HF and CIS levels. [b] The meanings of symbols can be found in Table 1. [c] C_{2v} structure with symmetrical O−S bonds. This structure was used to calculate topological properties at CIS. [d] C_S structure with unsymmetrical S−O bonds. This structure is only 19 cm^{-1} lower in energy than C_{2v} structure at EOM-CCSD/6-311++G(d,p) level.

that the unsymmetrical b_1 orbital may have less antibonding character during the excitation,[40] Innes suggested that coupling (perturbation theory) with the GS or a higher $^1A_1$ excited state better accounted for the unsymmetrical geometry of the AES.[41]

In this group of three triatomics, CS_2 differs from CO_2 and SO_2. The multiple bonds of CS_2 have more covalent character than the bonds of CO_2 and SO_2; in the case of the ground states, the C−S DIs (1.655) are significantly larger than the C−O (1.174) and S−O (1.221) DIs at the CCSD level. This value increases to 2.04 when the NMOs corresponding to the HF virtual space are set unoccupied at CCSD, confirming that the HF occupied space is the "normal" single determinant and the 'occupied' HF virtual space serves to include Coulomb correlation. When the same procedure is used for the ground states of CO_2 and SO_2 at CCSD, the C−O and S−O DIs increase slightly to 1.322 and 1.426, respectively. The more balanced treatment (including correlation) enables CCSD and EOM-CCSD to predict more accurate geometrical parameters than HF and CIS (Tables 5−7).

TABLE 8: The π Contributions to λ and δ for the $\tilde{C}^1B_2$ ($^1A'$) Excited State of SO_2 at Correlation Levels[a]

	GS	vertical excited state	adiabatic-TS	adiabatic excited state
λ	CCSD	EOM	EOM-TS[b]	EOM[b]
O	1.338	1.359	1.378[1.353]	1.471[1.449]
S	0.423	0.833	0.859[0.834]	0.827[0.802]
O	1.338	1.359	1.378[1.353]	1.289[1.264]
δ				
O−S	0.410	0.218	0.186[0.192]	0.272[0.279]
S−O	0.410	0.218	0.186[0.192]	0.127[0.132]
O,O	0.108	0.038	0.038[0.038]	0.037[0.038]
$\Sigma\lambda + 0.5\Sigma\delta$	4.027	4.026	4.025[3.962]	4.025[3.964]
		NMO Occupation Numbers		
a2	1.929	1.165	1.178	1.359
b1	0.088	0.840	0.803	0.635

[a] Please refer to Table 1 for notations. [b] Data in brackets calculated with all NMOs unoccupied except for the three mentioned in Figure 5. (a_2, b_1, and lower red line).

The smaller bond angle (105 vs 119°) and its unsymmetrical structure render the $\tilde{C}^1B_2$ ($^1A'$) excited-state of SO_2 interesting.[38] Because the π and π^* MOs are oriented perpendicular to the O−S−O plane it is possible to separate π contributions. There is another π-type MO (Figure 5, red line below a2) besides a_2 and b_1. The π contributions are given in Table 8. In going from the VES to the symmetrical AES, S LI increases slightly and the O LIs decrease although the π component of the O LIs increases slightly—data in the EOM-TS column of Table 7. The O−S DIs decrease from 1.012 to 0.978. This indicates that the net DI change is determined by π contributions (0.218 to 0.186). The 0.115 Å increase in S−O bond lengths contributes to the decrease in S−O DIs. Bending stabilizes (0.9 eV) the symmetrical AES. In going from the symmetrical AES to the unsymmetrical one, the changes in bond lengths produce an insignificant change in energy. If the reduced antibonding character of b_1 NMO is connected with the increase in the DIs, then the increase in the S−O DI (the sum is 1.991 relative to the sum of 1.956 for the symmetrical AES) might explain why the unsymmetrical structure exists, which is in accord with Mulliken's explanation. When only three NMOs are considered in π space, DI still increases (Table 8), i.e., the inclusion of other NMOs does not significantly alter the situation. Thus we conclude that the unsymmetrical AES is preferred due to the reduced antibonding character of b_1 NMO. This conclusion is further supported by the occupation numbers of the NMOs (Table 8). In going from the GS to the VES, the occupation number of b_1 (0.840) approaches 1, as expected for singlet excited state. When the VES relaxes to the AES the b_1 occupation number deceases, in fact, quite dramatically to 0.635 in achieving the unsymmetrical AES; the contribution of antibonding b_1 decreases as the unsymmetrical structure stabilizes AES.

It is noteworthy that the CO_2 (Table 5), CS_2 (Table 6), and SO_2 (Table 7) ground states exhibit significant DIs for the terminal pairs of atoms (HF 0.327, 0.382, and 0.336; CCSD 0.243, 0.285, and 0.258). In previous studies at HF and DFT levels, DIs of this magnitude for pairs of atoms separated by an atom have been interpreted as indicating 3c−4e bonding.[10,60] Our work shows that is also the case at correlation levels of theory, but with the CCSD DIs being smaller than the HF DIs. When all virtual space NMOs are set unoccupied, the CCSD DIs between the two terminal atoms increase to 0.342, 0.436, and 0.366 for CO_2, CS_2, and SO_2, respectively; the smaller values at CCSD derive from the Coulomb correlation effect. As seen for the C−X DIs, these DIs decrease in going to the excited states. The reason is similar to the correlation effect, since the excitations are also included in the consideration of correlation.

4. Discussion

We have discussed the LI and DI for the excited states, and the impact of Coulomb correlation on both LI/DI and structures. There are a few points we would like to clarify. (1) The molecules we studied are special cases. The studied excited states are all valence states, of which the excitation electronic extent is quite small, but the result structural distortion is significant. For these cases, we can derive most information of LI and DI simply based on two NMOs. The use of MO plots is rather heuristic than rigorous. (2) Our main purpose here is to show the applicability of our approach. More information might be obtained by the separation of α, β contributions,[59c] and the study of triplet excited states. (3) Two methods CIS and EOM-CCSD are based on single-reference; thus, we have unusual bond lengths for $\pi \rightarrow \pi^*$ of ethene due to the degeneracy of two states which may need multireference treatment. (4) Our approach is closely related to the progress of GAUSSIAN program packages, with the purpose to have a consistent procedure to analyze electronic density at different correlated levels. The approaches to analyze correlation effects might be different among different groups, but we believe that they compensate each other and give us better and better understanding of correlation effects.

As far as the chemical bond is concerned, one may define it by bond length and density distribution, both of which can be determined experimentally and theoretically. For the sake of vigorous analyses, we may calculate the density at the bond critical point (ρ_{BCP})[69] and delocalization indices (DI, δ) between atoms according to Bader's QTAIM theory. It is interesting to know the relationship among these parameters, thus we list the calculated values (bond length, ρ_{BCP}, DI) for the multiple bonds in Table S1−S7.

For GS (Tables S1−S3), CCE reduces the magnitude of both DI and ρ_{BCP} (CH_2S and CS_2 roughly keep the same ρ_{BCP} at both HF and CCSD levels). For 32 compounds containing a variety of chemical bonds, DI and ρ_{BCP} are found to have overall linear relationship—the correlation coefficients (r) are separately 0.902 and 0.928 at HF/6-311++G(2d,2p) and QCISD/6-311++G(2d,2p) levels of theory. The CCE generally gave larger percentage reduction for DI than for ρ_{BCP}. We also noticed that the molecules formed from second-row elements had DIs close to the molecules that include third-row elements in the same group, but the "second-row" molecules exhibited larger ρ_{BCP}s. This was explained on the basis of difference in bond lengths.[12b] For all the multiple bonds in the current study, ρ_{BCP} has very good linear relationship with bond length—r values are 0.998 and 0.999 at HF and CCSD levels, respectively. The corresponding r values for bond length and DI are separately 0.919

and 0.956 at HF and CCSD levels. The QCISD DI values are slightly smaller than CCSD ones due to marginally bigger π^* occupation numbers in the former method(Table S2 and Table S3).

The CCE will also reduce the magnitude of both DI and ρ_{BCP} in VES (Table S4 and Table S5). The DI magnitudes at CIS and at EOM-CCSD levels are closer together in comparison with GS values. For the occupancy of VES π^* NMOs is increased to be about 1.0, the DI is generally much smaller than that of GS. Though we may expect a similar decease of ρ_{BCP} in going from GS to VES, we notice that ρ_{BCP} is actually increased in covalent compounds such as $H_2C{=}CH_2$, $HC{\equiv}CH$, $H_2C{=}S$, and CS_2. This can be traced back to the character of π NMO. Because of the nodal plane containing the BCP, the π NMO has little contribution to the density at BCP; thus, the rearrangement of electron density in VES can possibly increase ρ_{BCP}.

The structures of AES suffer extensive distortions. The CCE will reduce the magnitude of ρ_{BCP} and DI as generally found (Table S6 and Table S7). Since the bond lengths are significantly stretched from VES to AES, the ρ_{BCP}s are reduced significantly. The DI magnitudes only change slightly from VES to AES. Though the magnitudes of DI are generally decreased, they increase when the distortion reduces the antibonding character of π^* NMO such as in cases of $H_2C{=}CH_2$ and SO_2.

To summarize, two parameters agree with each other very well in the analysis of chemical bonds. In the meantime, some unique features are also evident for different parameters. (1) ρ_{BCP} has excellent linear relationship with bond length for GS- (r values are 0.998 at HF level and 0.999 at CCSD level), VES (*r* values are 0.997 at CIS level and 0.999 at EOM-CCSD level), and AES (*r* values are 0.996 at CIS level and 0.998 at EOM-CCSD level). The small ρ_{BCP} values for AES are due to the significantly stretched multiple bonds. The π NMO contributes very little to ρ_{BCP} due to its nodal plane containing BCP, thus the vertical $\pi{\rightarrow}\pi^*$ excitation may even increase ρ_{BCP} in some cases ($H_2C{=}CH_2$, $HC{\equiv}CH$, $H_2C{=}S$ and CS_2). 2) The DI magnitudes can be tied up with the occupation number of π^* NMO, thus the DI magnitudes will be reduced dramatically for the correlated methods in comparison with HF and for the excited states in comparison with GS. The DI magnitudes can be increased if the antibonding character of π^* NMO is lessened (SO_2 and $H_2C{=}CH_2$).

5. Conclusions

We have successfully used AIM localization and delocalization indicies in the study of electronic excited states. The post-HF derivative method allows generalized density and diagonalized 1 reduced density matrices to be obtained at CIS and EOM-CCSD levels; wave functions are expressed in the format of natural orbitals in a single expanded determinant. The expansion of occupied space to the virtual space provides a practical way to study electron excitation and to include Coulomb correlation effects in ground states at correlated levels.

With the aid of Walsh diagrams and plots of molecular orbitals, we have been able to interpret AIM LIs and DIs in a three-dimensional sense. Phases revealed in MOs are carried to atomic overlap matrix (AOM) elements, and in turn are reflected in the calculated LIs and DIs. In our study, all molecules have multiple bonds, and the excitation to the immediate antibonding orbitals causes extensive structural changes, and also significantly reduces the DIs of multiple bonds. The partial occupation of the antibonding orbitals due to Coulomb correlation is also the reason why the ground state multiple bonds have significantly smaller DIs at correlated levels than at the HF level.

By comparing experimental and theoretical results, we established that Coulomb correlation is essential for obtaining results close to the experimental ones. In the meantime, AIM DIs calculated by conventional correlated methods may have noticeable changes from those at HF level (such as the significant decrease in multiple bond DIs)—a similar effect to the excited states, so it is likely that this will be also true for other parameters normally established at HF levels.

Acknowledgment. The work at Yale was supported by National Science Foundation Grant CHE-0445847. At McMaster it was supported by the Natural Sciences and Engineering Research Council of Canada (NSERCC). The authors also thank James R. Cheeseman of Gaussian, Inc., for assistance in obtaining wave functions in the Gaussian file format from the EOM-CCSD natural molecular orbitals.

Supporting Information Available: Tables of topological parameters. This material is available free of charge via the Internet at http://pubs.acs.org.

References and Notes

(1) Foo, P. D.; Inns, K. K. *J. Chem. Phys.* **1974**, *60*, 4582.
(2) Jensen, F.; Bunker, P. R. *J. Mol. Spectrosc.* **1982**, *94*, 114.
(3) Foresman, J. B.; Head-Gordon, M.; Pople, J. A.; Frisch, M. J. *J. Phys. Chem.* **1992**, *96*, 135.
(4) Dreuw, A.; Head-Gordon, M. *Chem. Rev.* **2005**, *105*, 4009.
(5) Bartlett, R. J.; Stanton, J. F. In *Reviews in Computational Chemistry*; Lipkowitz, K. B., Boyd, D. B., Eds.: VCH Publishers: New York, 1994; Vol. 5, p 65.
(6) Wiberg, K. B.; Wang, Y.-G.; de Oliveira, A. E.; Perera, S. A.; Vaccaro, P. H. *J. Phys. Chem. A* **2005**, *109*, 466.
(7) Bader, R. F. W. *Atoms in Molecules: A Quantum Theory*; Oxford University Press: Oxford, 1990.
(8) (a) Bader, R. F. W.; Stephene, M. E. *J. Am. Chem. Soc.* **1975**, *97*, 7391. (b). Bader, R. F. W.; Streitwieser, A.; Neuhaus, A.; Laidig, K. E.; Speers, P. *J. Am. Chem. Soc.* **1996**, *118*, 4959.
(9) Poater, J.; Duran, M.; Sola, M.; Silvi, B. *Chem. Rev.* **2005**, *105*, 3911. (b) Merino, G.; Vela, A.; Heine, T. *Chem. Rev.* **2005**, *105*, 3812.
(10) Fradera, X.; Poater, J.; Simon, S.; Duran, M.; Sola, M. *Theor. Chem. Acc.* **2002**, *108*, 214.
(11) Fradera, X.; Austen, M. A.; Bader, R. F. W. *J. Phys. Chem. A* **1999**, *103*, 304.
(12) (a) Wang, Y.-G.; Werstiuk, N. H. *J. Comput. Chem.* **2003**, *24*, 379. (b) Wang, Y.-G.; Matta, C. F.; Werstiuk, N. H. *J. Comput. Chem.* **2003**, *24*, 1720.
(13) (a) Fulton, R. L. *J. Phys. Chem.* **1993**, *97*, 7516. (b) Fulton, R. L.; Mixon, S. T. *J. Phys. Chem.* **1993**, *97*, 7530. (c) Fulton, R. L.; Mixon, S. T. *J. Phys. Chem.* **1995**, *99*, 9768.
(14) Stanton, J. F.; Gauss, J.; Perera, S. A.; Yau, A.; Watts, J. D.; Nooijen, M.; Oliphant, N.; Szalay, P. G.; Lauderdale, W. J.; Gwaltney, S. R.; Beck, S. R.; Balkova, A.; Bernholdt, D. E.; Baeck, K.-K.; Rozyczko, P.; Sekino, H.; Huber, C.; Pittner, J. P.; Bartlett, R. J. *ACES II*; University of Florida: Gainsville, FL, 2005.
(15) Keith, T. A. *AIMALL for SGI*; Yale University: New Haven, CT, 1996.
(16) Biegler-Konig, F. W.; Bader, R. F. W.; Tang, T.-H. *J. Comput. Chem.* **1982**, *3*, 317.
(17) Wang, Y.-G.; Werstiuk, N. H. *LI-DICALC*; McMaster University: Hamilton, Canada, 2002.
(18) (a) Hirota, E.; Endo, Y.; Saito, S.; Yoshida, K.; Yamaguchi, I.; Machida, K. *J. Mol. Spectrosc.* **1981**, *89*, 223. (b) Kuchitsu, K. *J. Chem. Phys.* **1966**, *44*, 906. (c) Berry, R. J.; Harmony, M. D. *Struct. Chem.* **1990**, *1*, 49.
(19) Foo, P. D.; Innes, K. K. *J. Chem. Phys.* **1974**, *60*, 4582.
(20) (a) Mulliken, R. S. *Rev. Mod. Phys.* **1942**, *14*, 265. (b) Merer, A. J.; Mulliken, R. S. *Chem. Rev.* **1969**, *69*, 639.
(21) Berry, R. J.; Harmony, M. D. *Struct. Chem.* **1990**, *1*, 49.
(22) Huet, T. R.; Godefroid, M.; Herman, M. *J. Mol. Spectrosc.* **1990**, *144*, 32.
(23) (a) Innes, K. K. *J. Chem. Phys.* **1954**, *22*, 863. (b) Ingold, C. K.; King, G. W. *J. Chem. Soc.* **1953**, 2702.
(24) Clouthier, D. J.; Ramsay, D. A. *Ann. Rev. Phys. Chem.* **1983**, *34*, 31.
(25) (a) Moule, D. C.; Walsh, A. D. *Chem. Rev.* **1975**, *75*, 67. (b) Walsh, A. D. *J. Chem. Soc.* **1953**, *2260*, 2603.
(26) Streitwieser, A.; Kohler, B. *J. Am. Chem. Soc.* **1988**, *110*, 3769.

(27) (a) Bruna, P. J.; Hachey, M. R. J.; Grein, F. *J. Mol. Struct.* **1997**, *400*, 177. (b) Duncan, J. L. *Mol. Phys.* **1974**, *28*, 1177.
(28) Jensen, P.; Bunker, P. R. *J. Mol. Spectrosc.* **1982**, *94*, 114.
(29) Cox, A. P.; Hubbard, S. D.; Kato, H. *J. Mol. Spectrosc.* **1982**, *93*, 196.
(30) Jensen, P.; Bunker, P. R. *J. Mol. Struct.* **1982**, *95*, 92.
(31) Ermakov, K. V.; Butayev, B. S.; Spiridonov, V. P. *J. Mol. Struct.* **1989**, *197*, 307.
(32) (a) Dixon, R. N. *Proc. Royal Soc. London, Ser. A* **1963**, *275*, 431. (b) Cossart-Magos, C.; Launay, F.; Parkin, J. E. *Mol. Phys.* **1992**, *75*, 835.
(33) Morino, Y.; Iijima, T. *Bull. Chem. Soc. Jpn.* **1962**, *35*, 1661.
(34) Jungen, C.; Malm, D. N.; Merer, A. J. *Can. J. Phys.* **1973**, *51*, 1471.
(35) Morino, Y.; Tanimoto, M.; Saito, S. *Acta Chem. Scand. A* **1988**, *42*, 346.
(36) Hoy, A. R.; Brand, J. C. D. *Mol. Phys.* **1978**, *36*, 1409.
(37) Ruedenberg, K. *Rev. Mod. Phys.* **1962**, *34*, 326.
(38) Katagiri, H.; Sako, T.; Hishikawa, A.; Yazaki, T.; Onda, K.; Yamanouchi, K.; Yoshino, K. *J. Mol. Struct.* **1997**, *413*−*414*, 589.
(39) Nachtigall, P.; Hrusak, J.; Bludsky, O.; Iwata, S. *Chem. Phys. Lett.* **1999**, *303*, 441.
(40) Mulliken, R. S. *Can. J. Chem.* **1958**, *36*, 10.
(41) Innes, K. K. *J. Mol. Spectrosc.* **1986**, *120*, 1.
(42) Buenker, R. J.; Peyerimhoff, S. D. *Chem. Rev.* **1974**, *74*, 127.
(43) Gillespie, R. J.; Popelier, P. L. A. *Chemical Bonding and Molecular Geometry: From Lewis to Electron Density*; Oxford University Press: Oxford, 2001.
(44) (a). Crawford, T. D.; Schaefer, H. F., III In *Reviews in Computational Chemistry*; Lipkowitz, K. B., Boyd, D. B., Eds.; VCH Publishers, Inc.: New York, 2000; Vol. 14, pp 33−136. (b). Bartlett, R. J.; Stanton, J. F. In *Reviews in Computational Chemistry*; Lipkowitz, K. B., Boyd, D. B. Eds. VCH Publishers, Inc.: New York, 1994; Vol. 5, pp 65−169.
(45) (a) Poater, J.; Sola, M.; Duran, M.; Fradera, X. *J. Phys. Chem. A* **2001**, *105*, 2052. (b) Poater, J.; Sola, M.; Duran, M.; Fradera, X. *J. Phys. Chem. A* **2002**, *106*, 4794.
(46) Foresman, J. B.; Schlegel, H. B. In *Recent Experimental and Computational Advances in Molecular Spectroscopy*; Fausto, R., Ed.; Kluwer Academic Publishers: Dordrecht, The Netherlands, 1993; pp 11−26.
(47) Wiberg, K. B.; de Oliviera, A. E.; Trucks, G. *J. Phys. Chem. A* **2002**, *106*, 4192.
(48) (a) Muller, A. M. K. *Phys. Lett.* **1984**, *105*, 446. (b) Goedecker, S.; Umrigar, C. J. *Phys. Rev. Lett.* **1998**, *81*, 866. (c) Holas, A. *Phys. Rev.* **1999**, *59*, 3454. (d) Cioslowski, J.; Pernal, K. *J. Chem. Phys.* **1999**, *111*, 3396.
(49) Buijse, M. A.; Baerends, E. J. *Mol. Phys.* **2002**, *100*, 401.
(50) Matito, E.; Sola, M.; Salvador, P.; Duran, M. *Faraday Discuss.* **2007**, *135*, 325, 367. DOI:10.1039/b605086g.
(51) Fulton, R. L. *J. Phys. Chem. A* **2006**, *110*, 12191.
(52) Cook, D. B. *Handbook of Computational Quantum Chemistry*, Oxford University Press, Oxford, **1998**, *pp285*−*295*.
(53) Levine, I. N. *Quantum Chemistry, Forth Edition*, Prentice Hall, Inc. Englewood Cliffs, New Jersey, **1991**.
(54) Poater, J.; Sola, M.; Duran, M.; Fradera, X. *Theor. Chem. Acc.* **2002**, *107*, 362.
(55) (a) Wang, L.-C.; Boyd, R. J. *J. Chem. Phys.* **1989**, *90*, 1083. (b) Boyd, R. J.; Wang, L.-C. *J. Comput. Chem.* **1989**, *10*, 367.
(56) (a) Handy, N. C.; Schaefer, H. F., III. *J. Chem. Phys.* **1984**, *81*, 5031. (b) Handy, N. C.; Amos, R. D.; Gaw, J. F.; Rice, J. E.; Simandiras, E. D. *Chem. Phys. Lett.* **1985**, *120*, 151. (c) Amos, R. D.; Rice, J. E. *Chem. Phys. Lett.* **1985**, *122*, 585. (d) Frisch, M. J.; Head-Gordon, M.; Pople, J. A. **1990**, *166*, 275. (e) Amos, R. D. *Chem. Phys. Lett.* **1980**, *73*, 602.
(57) Wiberg, K. B.; Hadad, C. M.; LePage, T. J.; Breneman, C. M.; Frisch, M. J. *J. Phys. Chem.* **1992**, *96*, 671.
(58) (a) Wiberg, K. B.; Hadad, C. M.; Foresman, J. B.; Chupka, W. A. *J. Phys. Chem.* **1992**, *96*, 10756. (b) Hadad, C. M.; Foresman, J. B.; Wiberg, K. B. *J. Phys. Chem.* **1993**, *97*, 4293. (c) Walters, V. A.; Hadad, C. M.; Thiel, Y.; Colson, S. D.; Wiberg, K. B.; Johnson, P. M.; Foresman, J. B. *J. Am. Chem. Soc.* **1991**, *113*, 4782.
(59) (a) Fulton, R. L. *J. Phys. Chem.* **1993**, *97*, 7516. (b) Fulton, R. L.; Perhacs, P. *J. Phys. Chem. A* **1998**, *102*, 9001. (c) Fradera, X.; Sola, M. *J. Comput. Chem.* **2002**, *23*, 1347.
(60) Molina, J. M.; Dobado, J. A. *Theor. Chem. Acc.* **2001**, *105*, 328.
(61) Matito, E.; Duran, M.; Sola, M. *J. Chem. Educ.* **2006**, *83*, 1243.
(62) Ponec, R.; Cooper, D. L. *Faraday Discuss.* **2007**, *135*, 31−42; 125−149.
(63) (a) Cioslowski, J., Eds. In *Many-Electron Densities and Reduced Density Matrices*; Kluwer Academic Press: Dordrecht, The Netherlands, 2000. (b) Cioslowski, J.; Buchowiecki, M.; Ziesche, P. *J. Chem. Phys* **2003**, *119*, 11570.
(64) Rablen, P. R.; Hadad, C. M. CASGEN, Yale University, 1994.
(65) Trucks, G. W. *Gaussian Inc.* Personal communication, 2007.
(66) Gatti, C.; MacDougall, P. J.; Bader, R. F. W. *J. Chem. Phys.* **1988**, *88*, 3792.
(67) Frisch, M. J.; Trucks, G. W.; Schlegel, H. B.; Scuseria, G. E.; Robb, M. A.; Cheeseman, J. R.; Montgomery, J. A., Jr.; Vreven, T.; Kundin, K. N.; Burant, J. C.; Millam, J. M.; Iyengar, S. S.; Tomasi, J.; Barone, V.; Mennucci, B.; Cossi, M.; Scalmani, G.; Rega, N.; Petersson, G. A.; Nakatsuji, H.; Hada, M.; Ehara, M.; Toyota, K.; Fukuda, R.; Hasegawa, J.; Ishida, M.; Nakajima, T.; Honda, Y.; Kitao, O.; Nakai, H.; Klene, M.; Li, X.; Knox, J. E.; Hratchian, H. P.; Cross, J. B.; Adamo, C.; Jaramillo, J.; Gomperts, R; Stratmann, R. E.; Yazyev, O.; Austin, A. J.; Cammi, R.; Pomelli, C.; Ochterski, J. W.; Ayala, P. Y.; Morokuma, K.; Voth, G. A.; Salvador, P.; Dannenberg, J. J.; Zakrzewski, V. G.; Dapprich, S.; Daniels, A. D.; Strain, M. C.; Farkas, O.; Malick, D. K.; Rabuck, A. D.; Raghavachari, K.; Foresman, J. B.; Ortis, J. V.; Cui, Q.; Baboul, A. G.; Clifford, S.; Cioslowski, J.; Stefanov, B. B.; Liu, G.; Liashenko, A.; Piskorz, P.; Komaromi, I.;. Martin, R. L.; Fox, D. J.; Keith, T.; Al-Laham, M. A.; Peng, C. Y.; Nanayakkara, A.; Challacombe, M.; Gill, P. M. W.; Johnson, B.; Chen, W.; Wong, M. W.; Gonzalez, C.; Pople, J. A. *Gaussian 03*; Gaussian, Inc.: Wallingford, CT, 2006.
(68) We might occasionally get small negative occupation numbers for the high NMOs. We can safely set them to be zero, because they are related to the contributions from highly excited determinants, whose contributions are normally negligible, and indeed they are very small in magnitudes.
(69) Wiberg, K. B.; Hadad, C. M.; Breneman, C. M.; Laidig, K. E.; Murcko, M. A.; LePage, T. J. *Science* **1991**, *252*, 1266.